Promotional effect of microwave radiation treatment on the desorption of CO_2 from mono-ethanolamine (MEA) solution over FeOOH catalyst

Haoran Zhang[1], Junge Lv[1], Zhibo Xiong[1]*, Huancong Shi[1], Jing Jin[1,4], Mengqi Liu[2], Yanping Du[3], Wei Lu[1]

1 School of Energy and Power Engineering, University of Shanghai for Science & Technology, Shanghai, 200093, China

2 School of Physics and Technology, University of Jinan, Jinan, 250022, China

3 School of Engineering, Lancaster University, Lancaster, LA1 4YW, UK

4. Shanghai Non-carbon Energy Conversion and Utilization Institute, Shanghai 200240, China

Abstract

Herein, microwave radiation had been applied to increase the catalytic desorption of CO_2 from CO_2-loaded MEA solution over the iron hydroxide catalyst, which was found to further accelerate the CO_2 desorption rate at the heating stage and decrease the relative desorption heat duty of FeOOH catalyst, and the M-FeOOH catalyst presents a good stability for CO_2 desorption. The treatment of microwave radiation leads to the decomposition of partial Fe-OH functional group of iron hydroxide and promotes the lattice transitions from β-FeOOH to α-FeOOH, which decreases the BET surface area and weak acid sites of FeOOH catalyst slightly, but increases the dispersion, medium-strong acid sites and pore volume of catalyst. Furthermore, this treatment reduces the calculated surface molar ratio of lattice hydroxyls/(lattice oxygen + lattice hydroxyls), but the cyclic test helps to the formation of hydroxyl oxygen from the adsorbed water, which plays an important role on the regeneration of MEA solution. The results of DFT calculation indicate that water molecule indeed contributes to converting the original intra-molecular proton transfer into the molecule-to-molecule proton transfer in the reaction of isomerization actively. Finally, the influence of iron-based catalyst on the isomerization of MEA solution are calculated by choosing Fe^{2+} of ferrous chloride as the unsaturated metal (LAS) active sites to simulate the adsorption of carbamic acid, and found that the adsorption of LAS and uniformly dispersed active sites of iron-based catalyst contributed to providing an advantageous condition for the decomposition of carbamate and promoting the regeneration of MEA.

* Corresponding author: Zhibo Xiong, Tel.: +86 21 55272320, Email addresses: xzb412@usst.edu.cn (Z.Xiong)

32   **1 Introduction**

33   The emission of carbon dioxide (CO_2) is bringing a critical environmental challenge that must

34   be addressed to achieve the sustainable development [1-3]. Carbon capture, utilization and storage

35   (CCUS) is crucial and effective in mitigating the global warming caused by CO_2 emission [4,5].

36   Among this, amine scrubbing is proven to be a handy and commercially available post-combustion

37   carbon capture (PCC) technology [6,7]. Furthermore, due to low cost and effectiveness, the mono-

38   ethanolamine (MEA) aqueous is currently the most representative solvent for the amine scrubbing

39   [5,8]. However, the high energy consumption is required for breaking the C-N bond of carbamate

40   ($RNHCOO^-$) in the CO_2-loaded MEA solution (ΔH = -84 kJ/mol), resulting in a high regeneration

41   temperature of 120-140 ^{o}C and the corresponding problems of water evaporation and amine corro-

42   sion, thereby hinders the large-scale commercial application of MEA solution for CO_2 capture [9-13].

43   Therefore, many methods, including temperature enhancement, pressure reduction, desorption op-

44   timization and catalytic desorption, have been proposed to reduce the regeneration energy consump-

45   tion for the CO_2-loaded MEA solution [14-18], but catalytic desorption is more conducive to balance

46   the high rate of desorption and the low energy consumption of regeneration.

47   Owing to abundant acid active sites and large surface area, the solid acid catalyst (SAC) has

48   been widely used to the low-temperature regeneration of CO_2-loaded MEA solution by facilitating

49   the decomposition of carbamate and the regeneration of protonated amines, which increased the

50   desorption rate of CO_2 and reduced the regeneration energy consumption significantly [19,20,21].

51   Wherein, the abundant acid sites of catalyst are conducive to break the C-N bond of carbamate by

52   providing protons for its decomposition directly, and large specific surface area helps shorten the

53   reaction pathway by exposing more active sites to anchor the carbamate [18,22,23]. Metal oxides have

54   been widely used as commercially viable catalysts caused by the ease synthesis, low cost and large

55   acidic sites [23]. Bhatti et al. investigated the catalytic performance of metal oxides catalysts on CO_2

56   desorption from CO_2-loaded MEA solution and found that the MoO_3, ZrO_2 and Ag_2O catalysts with

57   more abundant acid sites presented superior catalytic performance and better stability than Cr_2O_3

58   and TiO_2 [24-26]. The natural clay materials, molecular sieves and activated carbon with rich pore

59   structure and high specific surface area have been used as carriers to improve the dispersion of metal

60 oxides [19,27,28]. For instance, the combined SnO_2/ATP catalyst increased the desorption rate and

61 amount of CO_2 by 265% and 222%, and reduced the relative heat duty by approximately 52% com-

62 pared to catalyst-free. But the catalytic performance of 1/2-SnO_2/ATP decreased by around 20%

63 after 12 cycles [19]. Similarly, Fe, Al, Mo-modified MCM-41 acid-base bi-functional catalysts also

64 presented good catalytic performance and increased the desorption factor of CO_2 by 206.3% to

65 337.1%. However, only 80% of the activity retained after five cycles, thus the maintaining stability

66 of catalyst in high alkalinity still needs to be resolved during the cycling experiments. Due to the

67 flexible design-ability, uniform porosity and unique chemical structure, metal organic framework

68 (MOF/COF) also has attracted a lot of attention in the catalytic desorption of CO_2 [23], and its com-

69 posite catalyst composed with transition metals exhibited excellent catalytic performance of CO_2

70 desorption [29]. It should be mentioned that the high synthesis cost and the restriction of large-scale

71 production makes the metal-organic backbone materials difficult to be applied commercially, alt-

72 hough they exhibit excellent cycling stability for the CO_2 desorption from amine solution. Further-

73 more, in order to improve the catalytic performance of CO_2 desorption, the surface modification of

74 sulfonation has been introduced to promote the acid sites of SAC catalyst, but due to the unstable

75 characteristics of the introduced acid sites, the stability of modified catalyst in high alkaline amine

76 is still a research hotspot for the desorption of CO_2 from MEA solution [5,32].

77   On account of the abundant active sites, metal hydroxides also present excellent catalytic per-

78 formance and stability in high alkaline amine for CO_2 desorption from amine solutions, especially

79 the amorphous samples with a large specific surface area, whose adsorption to the three active sites

80 exposed by carbamate is nonnegligible. The synthesized $TiO(OH)_2$ from isopropanol titanium pre-

81 sented the enhancement of 75% and more than 4500% respectively in the desorption amount and

82 rate of CO_2 from MEA solution, attributing to the accelerating protonation and de-protonation pro-

83 cesses from the -OH groups of $TiO(OH)_2$ basic oxide [31], and the hydroxyl groups of AlOOH had

84 also been confirmed to present similar promotional effect [32]. Furthermore, the hydroxide catalysts

85 of FeOOH and ZrOOH had no effect on the absorption of CO_2 during the cyclic experiment and

86 reduced the desorption heat duty by 47% and 45%, respectively [33]. Accordingly, metal hydroxides

87 exhibit a good potential in the catalytic desorption of CO_2 from amine solution, but the catalytic

88 mechanism is not comprehensively clear and needs to be studied further. Among the investigated

89 metal hydroxides, iron is a low-cost and environmentally friendly element, and iron-based catalysts

90   was regarded as an ideal candidate that has abundant acid sites, rich oxygen vacancies and good

91   electron transfer via the conversion of Fe(III)/Fe(II) [34], all of which are crucial properties in the

92   catalytic desorption of CO_2. However, the catalytic activity of FeOOH hydroxide still needs to be

93   further optimized before the application in the industrial desorption of CO_2 from amine solution.

94   Simultaneously, the intrinsic catalytic mechanism of CO_2 desorption over it is unclear and needs to

95   be investigated at the molecular levels by combining the quantitative and qualitative analysis of

96   acidic sites.

97   Microwave radiation can lead to a homogeneous rapid heating of the reaction medium, result-

98   ing in a blooming of nucleation, which is favorable to the formation of the synthesized sample with

99   a small particle size and a narrow particle size distribution [35,36]. As a result, microwave radiation

100 has been used to synthesize novel catalysts and exhibits a good reaction selectivity, which is con-

101 sidered to regulate the morphology of catalysts and improve the dispersion of active sites on the

102 surface [37]. Our previous studies demonstrated that the hydrothermal treatment of microwave radi-

103 ation was conducive to adjust the microscopic pore structure of iron-cerium-titanium mixed oxide

104 catalysts through accelerating the crystallite rate of the co-precipitated precursors, which also en-

105 larged the pore diameter and pore volume of the catalyst and enhanced its surface acid sites, thereby

106 increased the low-temperature SCR activity of mixed oxide catalyst [35]. Therefore, the treatment of

107 microwave radiation might refine the particle size of iron hydroxide and extend its specific surface

108 area and acid sites, resulting in improvement of CO_2 desorption from MEA solution over the iron-

109 based hydroxide catalyst.

110   In this research, microwave radiation was firstly employed to fabricate the catalyst of M-

111 FeOOH for the desorption of CO_2 from MEA solution, and the results indicate that the treatment of

112 microwave radiation improves the catalytic performance of CO_2 desorption, and the synthesized M-

113 FeOOH catalyst exhibits a good stability in high alkaline environments. Furthermore, various char-

114 acterization techniques, including SEM, XRD, FT-IR, XPS, BET, CO_2-TPD and Py-IR, were meas-

115 ured to investigate the influence of microwave radiation treatment on the physical-chemical prop-

116 erties of FeOOH catalyst. In addition, Gaussian 16W was used to study the isomerization of car-

117 bamic acid to zwitterion during the regeneration of MEA solution, highlighting the importance of

118 iron-based SAC catalyst in the adsorption of carbamate in this process. This research offers a cost-

119 effective and efficient method for the fabrication of catalyst used in the desorption of CO_2 and the

120 regeneration of adsorbed amine.

121 **2 Experimental section**

122 **2.1 Catalyst preparation**

123   All reagents used were of analytical grade (AR) and employed without further purification.

124 The M-FeOOH nano-catalysts were synthesized by the microwave-assisted precipitation method

125 using a home microwave oven (EG823MF3-NW, Midea, China). Initially, a certain quality of

126 $Fe(NO_3)_3 \cdot 9H_2O$ was dissolved in deionized water to achieve a solution concentration of 0.5 mol/L

127 for Fe^{3+}. The pH of the mixed solution was adjusted to 8 ~ 9 using ammonia, followed by continuous

128 stirring for 2 h. Subsequently, the mixture was filtered and washed extensively with deionized water

129 to remove NO_3^- and NH_4^+ ions. The resulting wet filter cake was vacuumed and then subjected to

130 microwave radiation treatment for 10 minutes, utilizing an alternating heating method of P_{30}, which

131 involves 8 seconds of microwave radiation followed by a 14-seconds pause, repeated in cycles.

132 Finally, the filter cake treated by microwave radiation was dried at 105 °C for 2 h. The catalyst

133 obtained through this process is designated as M-FeOOH. In order to reveal the influence of micro-

134 wave radiation treatment on the catalytic desorption of CO_2 from MEA solution over goethite, for

135 comparison, the vacuumed filter cake was directly dried at 105 °C for 2 h without the treatment of

136 microwave radiation, and the obtained catalyst is referred to FeOOH. Furthermore, the used M-

137 FeOOH catalyst after five cyclic tests is marked as Spent-M-FeOOH.

138 **2.2 Characterization methods**

139   The XRD pattern was obtained using an X-ray diffractometer (Rigaku smartlab, Japan Science)

140 with Cu Kα radiation (λ = 0.15406 nm), over a 2θ range from 20° to 80° at a scanning rate of 2 °/min,

141 under operating conditions of 40 kV and 40 mA. The N_2 adsorption-desorption isotherm at 77 K

142 was measured with a Micromeritics ASAP 2460 system. The Brunauer-Emmett-Teller (BET)

143 method was employed to determine the specific surface areas, while the pore size distributions of

144 catalysts were analyzed using the Barrett-Joyner-Halenda (BJH) method. X-ray photoelectron spec-

145 troscopy (XPS) was conducted on Thermo-Fisher Scientific Escalab250Xi (USA) with 150W mon-

146 ochromated Al Kα radiation (1486.6 eV), using the C 1s peak (binding energy=284.8 eV) to cali-

147 brate the binding energies of Fe 2p and O 1s. The base pressure in the analysis chamber was ap-

148 proximately 3×10^{-10} mbar. Fourier transform infrared (FTIR) spectra, spanning from 400 to 4000

149 cm^{-1}, were recorded using a Nicolet iS5 FTIR spectrometer with a resolution of approximately 4

150   cm^{-1}. The pyridine adsorption infrared spectroscopy (Py-IR) was obtained using a Thermo Nicolet

151   380 spectrometer to assess the acid sites of catalysts. Before pyridine adsorption, the samples were

152   pretreated at 105 °C under vacuum conditions and subsequently cooled to room temperature. A he-

153   lium flow of 20 mL/min, saturated with pyridine, was then introduced into the IR cell at room tem-

154   perature for 2 h to ensure the complete coverage of all acid sites. Following this, pyridine desorption

155   was performed by evacuating the cell for 30 minutes under vacuum at 150 °C and 250 °C, respec-

156   tively. Infrared spectra were collected at these specific temperatures. The particle size distributions

157   of catalysts were measured by three times with Malvern 2000, and CO_2-TPD was conducted on an

158   Auto Chem II 2920 analyzer (Micromeritics, USA). Under He atmosphere (30 mL/min), the tem-

159   perature is raised to 200 °C at the heating rate of 10 °C /min, The heat temperature is kept for 30 min

160   to remove the impurity water on the surface of the sample. After being cooled to 50 °C in He atmos-

161   phere (30 mL/min), high purity CO_2 gas (40 mL/min) is switched into the cell for 60 min and then

162   the purge of He gas (30 mL/min) is used to blow away the physically adsorbed CO_2 on the sample

163   surface for 30 min. Finally, the CO_2-TPD desorption is carried out from 50-500 °C at a heating rate

164   of 10 °C/min under the condition of He gas (30 mL/min).
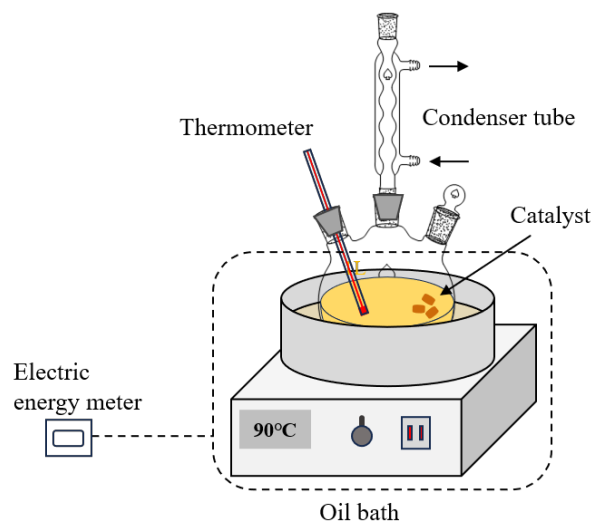
165

166   **Fig.1** Schematic diagram of catalytic desorption of CO_2 from MEA solution

167   **2.3 Absorption and desorption experiments**

168   The experiments of CO_2 absorption/desorption and repetitive testing were conducted in a semi-

169   intermittent device. For the absorption of CO_2, as shown in Fig. S1, pure CO_2 gaseous was passed

170   through the gas mass flow meter, three-way valve and wash flask at a rate of 1.5 L/min into a three-

171   necked flask containing 500 mL of a 30 wt.% MEA solution. And the water bath temperature was

172   maintained at 40±1 °C and the magnetic stirrer was set to 300 r/min during the absorption of CO_2

173   [17,26]. In order to monitor the adsorption of CO_2, a timer was employed and 1-1.5 mL of the absor-

174   bent solution was pipetted and collected into small bottles every 2-3 minutes throughout this time.

175   Furthermore, a bypass had been designed in the gas pathway of the semi-intermittent device and

176   was briefly paused to separate the pipetting procedure from the absorption process of CO_2. The

177   process of CO_2 absorption and sampling was set as follows: pure CO_2 gaseous at a fixed flow rate

178   was fed into the reactor directly by closing the valve of the bypass during the absorption of CO_2

179   absorption, while this valve was opened to divert the gaseous of pure CO_2 to the exit in the next

180   pipetting stage. And this interruption contributes to pipette 1-2 mL of the absorbed amine solution

181   for storage from the top of the reactor by halting the flow of CO_2 gas in the reactor temporarily.

182   Afterwards, the valve of the bypass was closed again to resume the absorption process by reintro-

183   ducing the gas flow of pure CO_2 into the reactor, ensuring the loading of CO_2 in MEA solution is

184   0.50 mol CO_2/mol amine, which was determined using a Chittick apparatus in Fig.S2.

185   For the desorption of CO_2, as shown in Fig.1, the experiments were performed in a 1 L three-

186   necked flask equipped with a thermometer, condenser tube and sampler. In each experiment, 2 g of

187   catalyst was immersed into the above CO_2-loaded MEA solution, and the desorption temperature

188   was maintained at 90±1 °C with a stirring of 400 r/min [18,32]. Furthermore, black thermal insulation

189   cotton was used around and above the oil bath to heat preservation for the accurate measurements.

190   When the temperature of MEA solution reached 40 °C, 1-1.5 mL of MEA solution was pipetted for

191   a Chittick titration to obtain the loading of CO_2 in the amine-enriched solution, and then this sam-

192   pling operation was carried out in next every five minutes, but the time intervals were kept at 15

193   min from 30 min to 60 min and then 30 min from 60 min to 120 min during the titration measure-

194   ment, respectively. At the same time, the power consumption was recorded using an energy meter.

195   The measured volume of CO_2 and the used volume of hydrochloric acid in the Chittick titration

196   were used to calculate the loading rate of CO_2, as described by the following equation.

197
$$\alpha = \frac{V_{CO2} - 2V_{HCl}}{V_{HCl} \times \zeta} \tag{1}$$

198   Where α is the calculated loading of CO_2, V_{CO2} is the released volume of CO_2, V_{HCl} is the

199   consumed amount of hydrochloric acid in the acid-base titration when the color of the titrated amine

200   aqueous solution changes completely and ζ is the gas correction factor calculated via the equation

201   of $\zeta = \dfrac{(T+273.15) \times 22.4}{273.15}$.

202   With respect to the catalytic desorption of CO_2 from MEA solution, the tested catalyst was

203   pressed into a thin flake and wrapped in a fine pore gauze mesh, which was effective to be used in

204   the middle portion of the CO_2-loaded MEA solution as illustrated in Fig.1. At the same time, ap-

205   proximate 12 pipetting operations need to be carried out for each experiment of CO_2 desorption,

206   resulting in a solvent loss of around 20-30 mL for MEA solution. This corresponds to around 4%-

207   6% solvent loss of its initial 500 mL. It was pointed out in previous research that the main factor

208   affecting the desorption rate(r) of CO_2 is the concentration of MEA^+COO^- in the CO_2-loaded MEA

209   solution [38]. Therefore, 4%-6% solvent loss of MEA solution has an insignificant impact on the

210   desorption rate of CO_2 due to no changing of amine concentration [24].

211   In this study, the desorption profiles of CO_2 loadings (mol/mol) versus time (minutes) were

212   plotted, ranging from saturation to equilibrium (0.5 mol/mol) for MEA solvents. And these CO_2

213   loadings were tested at least twice to ensure an average absolute deviation (AAD) below 5%. Fur-

214   thermore, the parameters for evaluating the desorption performance of CO_2, including the desorbed

215   quantities of CO_2 (n_{CO2}), the average desorption rate (r), the relative heat duty (RHD), the heat duty

216   (HD), the cycle capacity and the desorption parameter (DP) with the detailed definitions, are calcu-

217   lated as follows:

218
$$n_{CO_2} = C \times V \times \left(\alpha_{rich} - \alpha_{lean}\right) \tag{2}$$

219
$$r = \frac{n_{CO2}}{dt} = \frac{C \times V \times \left(\alpha_{rich} - \alpha_{lean}\right)}{dt} \tag{3}$$

220
$$HD = \frac{Q_{input}}{n_{CO2}} = \frac{kJ/h}{mol/h} \tag{4}$$

221
$$RHD = \frac{HD_i}{HD_{baseline}} \times 100\% \tag{5}$$

222
$$Cyclic\ capacity = C \times \left(\alpha_{rich} - \alpha_{lean}\right) \tag{6}$$

223
$$Desorption\ parameter = \frac{initial\ desorption\ rate \times cyclic\ capacity}{heat\ duty} \tag{7}$$

224   **2.4 Molecular simulation**

225   The calculations were performed based on the Gaussian 16W chemical calculation package.

226 To account for the solvent effects, the integrated equation formalism polarized continuum model

227 (IEFPCM) was employed, with the atomic radius being a critical parameter for the accuracy of the

228 solvation model. Pauling atomic radii was used to calculate reaction capacities and other properties.

229 Geometric optimizations were performed at the B3LYP/6-311G (d, p)/IEFPCM level. Energies were

230 calculated as single-point energies using the B3LYP/def2-TZVP/IEFPCM method. To investigate

231 various mechanisms, the Gaussian 16W algorithm with opt= (TS, calcafa, noeigen) was used to

232 identify transition states (TS). Reaction pathways were refined through the intrinsic reaction coor-

233 dinate (IRC) calculations to ensure the consistent methodology and basis sets with the transition

234 states (TS). Transition states (TS) were confirmed by vibrational frequency calculations, requiring

235 at least one imaginary frequency, and two energy minimization runs using the software's default

236 convergence conditions. IRC calculations were performed to determine the relationship between

237 transition states and local minima, analyzing the reactants, products, intermediates, transition state

238 structures and vibrational frequencies.

239 **3 Results and discussion**

240 **3.1 Catalyst characterization**

241 According to the XRD patterns of FeOOH, M-FeOOH and Spent-M-FeOOH catalysts as

242 shown in Fig.2(a), no typical sharp lattice diffraction peaks attributed to iron oxide or/and hydroxide

243 have been detected for these catalysts, but some broad background signals appear in the samples.

244 This suggests that iron-based crystals might mainly exist in an amorphous phase with an indetermi-

245 nate morphology or/and micro-crystals that cannot be detected. For the FeOOH catalyst, the de-

246 tected broad background signals of XRD patterns might be attributed to α-FeOOH (JCPDS No.29-

247 0713) and β-FeOOH (JCPDS No.34-1266), indicating that the precipitation of ammonia helps ob-

248 tain the amorphous/micro-crystal iron hydroxide catalyst, which had been confirmed to have a large

249 specific surface area, pore volume and abundant surface functional groups [29,31,34]. Interestingly, the

250 M-FeOOH catalyst treated by microwave radiation also presents the XRD patterns attributed to the

251 amorphous/micro-crystal α-FeOOH and β-FeOOH, but this treatment promotes the lattice transi-

252 tions from β-FeOOH to α-FeOOH. Previous researches pointed out that both α-FeOOH and β-

253 FeOOH presented good stability in alkaline environments, and the conversion of β-FeOOH to α-

254 FeOOH contributed to resulting in more hydroxyl groups formed on the as-prepared iron hydroxide

255 surface, which might facilitate the supply of protons to the carbamate, thus accelerating the regen-

256 eration of CO_2-loaded MEA solution. Furthermore, the co-presence of β-FeOOH and α-FeOOH

257 helps optimize the electronic structure of iron hydroxide catalyst, which might accelerate the elec-

258 tron transfer during the desorption of CO_2 from CO_2-loaded MEA solution [34,39]. The Spent-M-

259 FeOOH catalyst after five cyclic tests also exhibits the XRD patterns of iron hydroxide micro-crys-

260 tals similar to M-FeOOH, and α-FeOOH is the predominant crystal for the catalyst treated by mi-

261 crowave radiation. This indicates that the treatment of microwave radiation contributes to fabricat-

262 ing the iron hydroxide catalyst with good stability α-FeOOH as the predominant crystal.
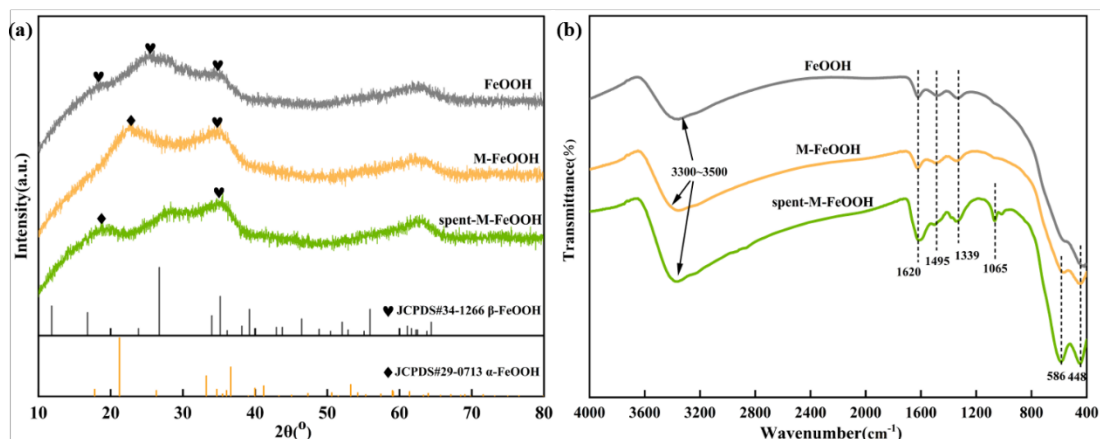
Fig.2 The XRD patterns (a) and FT-IR spectrums (b) of FeOOH, M-FeOOH and Spent-M-FeOOH catalysts

265 Fig.2(b) illustrates the surface functional groups of FeOOH, M-FeOOH and Spent-M-FeOOH

266 catalysts detected by FT-IR, and it is found that FeOOH and M-FeOOH catalysts present similar

267 FT-IR spectra, which are attributed to the stretching and bending vibrations of the OH groups of the

268 physically adsorbed water molecules on the catalysts surface(3356 cm^{-1} and 1620 cm^{-1}), the asym-

269 metric and symmetric stretching vibrations of Fe-O-H(1495 cm^{-1} and 1339 cm^{-1}) and the stretching

270 vibrations of Fe-O (586 cm^{-1} and 448 cm^{-1}) [30,40,41], respectively. This reconfirms that the treatment

271 of microwave radiation doesn't dehydrate goethite completely, and iron hydroxide still exists in the

272 M-FeOOH catalyst. Furthermore, the FT-IR spectrum of Spent-M-FeOOH catalyst is similar to

273 those of M-FeOOH with a stronger intensity, which might be attributed to the absorption of water

274 from MEA solution. It should be pointed out that a new narrow peak appears at 1065 cm^{-1} for the

275 Spent-M-FeOOH catalyst, attributing to the surface residual MEA. Therefore, the results of XRD

276 and FT-IR all demonstrate that microwave radiation treatment doesn't dehydrate the synthesized

277 goethite completely, and the M-FeOOH catalyst presents abundant OH groups with good stability,

278   which are highly favorable to the decomposition of carbamate.
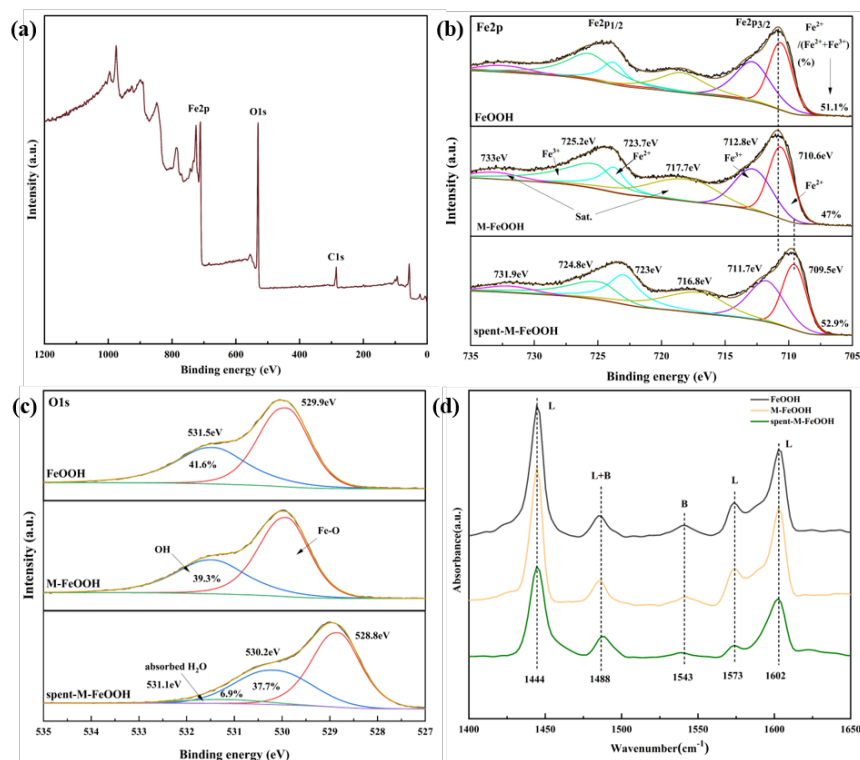

Fig.3 The XPS and Py-IR spectra of FeOOH, M-FeOOH and Spent-M-FeOOH catalysts: (a) Survey scanning

spectrum (b) Fe 2p spectrum (c) O 1s spectrum (d) The desorption spectra of pyridine at 150 °C

X-ray photoelectron spectroscopy (XPS) of FeOOH, M-FeOOH and Spent-M-FeOOH cata-

lysts were measured to investigate the dispersion of elements on the catalysts surface, and the results

are given in Fig.3. According to the full spectrum of XPS spectra in Fig.3(a), it is clear that the XPS

spectra of Fe 2p and O 1s are detected on the catalysts surface apart from C 1s, indicating that the

micro-crystals of α-FeOOH or/and β-FeOOH might be formed on the catalysts surface in view of

the fact that hydrogen cannot be detected by XPS. As shown in Fig.3(b), four peaks located at about

710.8 eV, 717 eV, 724.2 eV and 733 eV, were detected for the Fe 2p XPS spectra of FeOOH, M-

FeOOH and Spent-M-FeOOH catalysts. Except for two satellite peaks, the first and third peaks are

attributed to Fe $2p_{3/2}$ and Fe $2p_{1/2}$, respectively, which can be further de-convoluted into four peaks

via the Lorentz/Gaussian method due to their asymmetry [34,43]. This also validates the formation of

partial Fe^{2+} species on the catalysts surface. Interestingly, the treatment of microwave radiation does

not cause any shift in binding energies of Fe $2p_{3/2}$ and Fe $2p_{1/2}$, but it reduces the calculated

$Fe^{2+}/(Fe^{2+}+Fe^{3+})$ molar ratio on the surface of FeOOH catalyst by 4.1%, which indicates that the

treatment of microwave radiation can affect the interaction between iron and oxygen elements in

296 catalyst, thereby changes the electron cloud distribution of Fe. However, the cyclic tests for five

297 times lead around 1.1 eV of Fe 2p spectra to lower binding energy, indicating an increase in the

298 electron cloud density around iron, which might be attributed to the absorption of water or/and the

299 residual MEA on the catalyst surface. Furthermore, Spent-M-FeOOH presents a larger surface

300 $Fe^{2+}/(Fe^{2+}+Fe^{3+})$ molar ratio than FeOOH and M-FeOOH catalysts. Theoretically, the presence of

301 Fe^{2+} can facilitate the formation of oxygen vacancies due to the process 2 $Fe^{3+} \rightarrow Fe^{2+} + VO$ [34].

302 And this phenomenon is also evidenced by the XPS spectrum of O1s in this research. As shown in

303 Fig.3(c), the peaks located at about 529.9 eV and 531.5 eV are associated with the lattice oxygen

304 and the lattice hydroxyls, respectively [44]. Similar to the decrease law of surface $Fe^{2+}/(Fe^{2+}+Fe^{3+})$

305 molar ratio, the treatment of microwave radiation also reduces the calculated molar ratio of lattice

306 hydroxyls/(lattice oxygen+lattice hydroxyls) by 2.3%. Meanwhile, five cyclic tests lead to a new

307 peak appear at around 531.2 eV, which is attributed to hydroxyl oxygen from the adsorbed water,

308 and the total molar ratio of lattice hydroxyls and hydroxyl oxygen of Spent-M-FeOOH is higher

309 than that of M-FeOOH catalyst. This indicates that the cyclic tests contributes to improve the surface

310 concentration of oxygen vacancies due to the adsorption of H_2O, which also leads the O1s energy

311 spectrum shift to the lower binding energy by 1 eV in agreement with the observation for Fe 2p.

312 Based on the following catalytic activity of CO_2 desorption from MEA solution in section 3.2, it can

313 be inferred that the oxygen vacancies might play an important role on the catalytic desorption of

314 CO_2 over FeOOH catalyst, but it is not the dominant factor in this circumstance.

315 　　In order to investigate the influence of microwave radiation treatment on the Brønsted and

316 Lewis acid sites of FeOOH catalyst, a Py-IR study was conducted and the results are given in Fig.4

317 and Table 1. From Fig.4, it can be found that five peaks are detected for FeOOH, M-FeOOH and

318 Spent-M-FeOOH catalysts. Among them, the peaks located at 1444 cm^{-1}, 1573 cm^{-1} and 1602 cm^{-1}

319 are attributed to Lewis acid sites (L), and the peaks located at 1543 cm^{-1} and1488 cm^{-1} belong to

320 Brønsted acid sites (B) and the combination of L and B acid sites, respectively [30,45,46]. Thus, there

321 exists abundant weak and medium-strong acid sites for the as-prepared iron hydroxide catalyst, and

322 the treatment of microwave radiation doesn't affect the strength of acid sites of FeOOH. The calcu-

323 lated values of Lewis and Brønsted acid sites from the Py-IR curves at 150 $^{\circ}C$ and 250 $^{\circ}C$ in Table

324 1 demonstrate that the treatment of microwave radiation decreases the amount of weak acid sites of

325 FeOOH catalyst slightly, but it increases the amount of medium-strong acid sites of catalyst [47]. And

326   the reasons that the slight decrease of total acid sites might be attributed to the desorption and de-

327   composition of partial Fe-OH functional group during the treatment of microwave radiation, which

328   is also supported by the calculated molar ratios of L/B for both weak and medium-strong acid sites

329   and is in accordance with the results of XPS spectra. It should be mentioned that after five cyclic

330   tests, the Spent-M-FeOOH catalyst exhibits much less weak and medium-strong acid sites than M-

331   FeOOH, attributed to the surface residue of MEA, although the obtained Spent-M-FeOOH catalyst

332   was washed thoroughly with de-ionized water. Meanwhile, the spent catalyst has a larger calculated

333   molar ratio of L/B for weak acid sites than those of FeOOH and M-FeOOH, which indicates Lewis

334   acid sites are well reproducible in the catalytic desorption of CO_2, whereas the calculated molar

335   ratio of L/B at medium-strong acid sites decreases more. In particular, the reduction intensity of B

336   acid sites is lower than those of L acid sites during the cyclic test, suggesting that the surface hy-

337   droxyl groups are stable in high alkaline environments [32], which is in agreement with the results of

338   XPS spectroscopy. Therefore, the repetitive testing not only decreases the BET surface area of M-

339   FeOOH catalyst, but also reduces the amount of the total acid sites, especially. It is widely accepted

340   that the amount of surface acid sites is related to the intrinsic properties and specific surface area of

341   catalyst, thus the normalizations of acid sites over per specific surface area (Acidity) were calculated

342   to study the inherent acidity of the catalysts and the results are also given in Table 1 [47]. It can be

343   found that Spent-M-FeOOH presents the largest calculated amount of acidity for weak acid sites,

344   indicating that the Spent-M-FeOOH catalyst still has abundant weak acidic sites over per specific

345   surface area, although its BET surface area is the least among these characterized catalysts. In order

346   to study the effect of microwave radiation treatment on the surface active sites of catalyst, CO_2-TPD

347   was used to qualitatively compare the amount of hydroxyl active sites on the surface of FeOOH and

348   M-FeOOH catalysts, and the results are given in Fig.S4. As depicted in Fig. S4, there exists an

349   obvious desorption peak around 81 °C for FeOOH and M-FeOOH catalysts, which is attributed to

350   the decomposition of the generated bicarbonates during the adsorption of CO_2 on the surface hy-

351   droxyl groups of catalysts [32]. But the treatment of microwave radiation reduces the amount of -OH

352   species on the FeOOH catalyst surface, which confirms the influence of microwave radiation treat-

353   ment on reducing partial hydroxyl groups of FeOOH catalyst again.

354
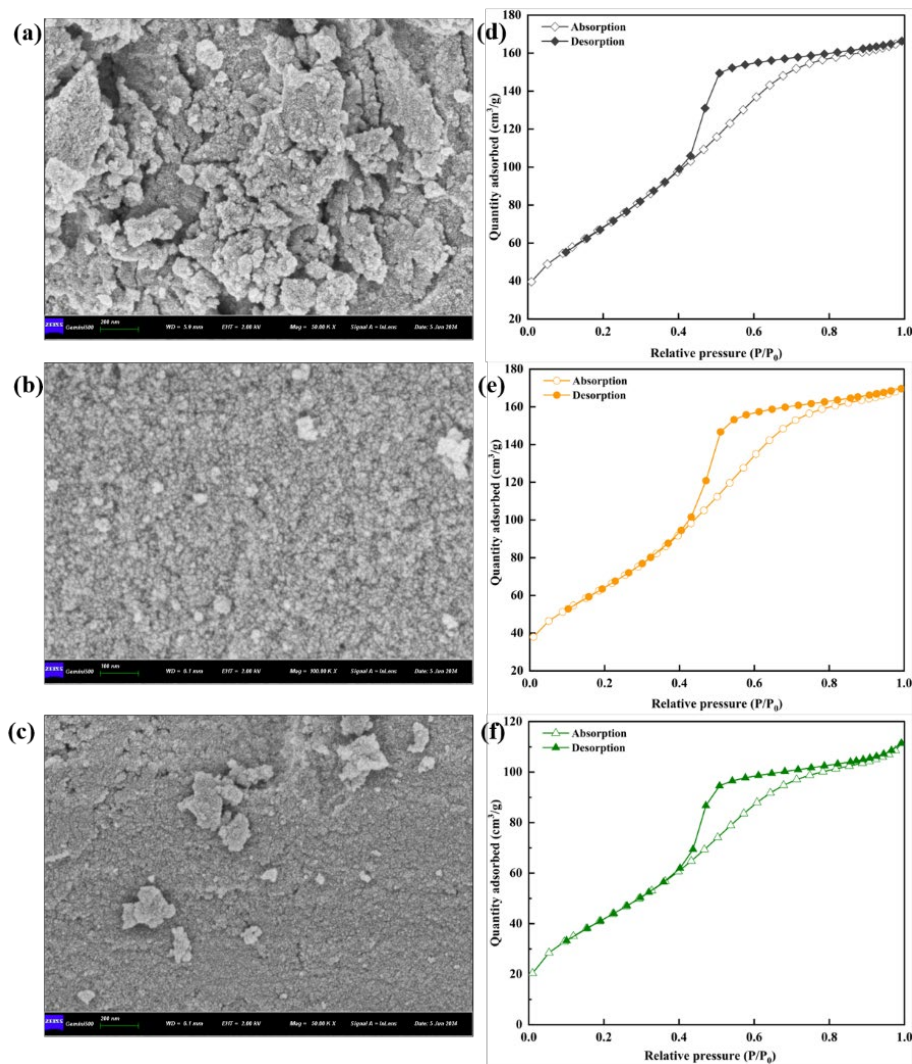
Fig.4 The SEM images of (a) FeOOH (b) M-FeOOH (c) Spent- M-FeOOH catalysts and Corresponding N$_2$ ad-

sorption-desorption isotherms (d-f)

Table 1 The concentrations and distributions of Lewis (L) and Brønsted (B) acid sites for FeOOH, M-FeOOH and

Spent-M-FeOOH catalysts

Samples	Weak acid (mmol/g)					Medium-strong acid (mmol/g)				
	B	L	L/B	Total	Acidity[a] (umol/m^2)	B	L	L/B	Total	Acidity[a] (umol/m^2)
FeOOH	0.024	0.198	8.13	0.223	0.86	0.016	0.116	7.13	0.132	0.51
M-FeOOH	0.022	0.180	8.20	0.202	0.84	0.015	0.119	7.80	0.134	0.56
Spent-M-FeOOH	0.013	0.147	11.12	0.160	0.99	0.01	0.066	6.72	0.075	0.47

[a] Calculated from the acid amount per S$_{BET}$ of the samples

Fig.4 (a)-(c) shows the SEM photographs of FeOOH, M-FeOOH and Spent-M-FeOOH cata-

361 lysts, and it can be observed that the FeOOH catalyst displays a large clump shape with tight inter-

362 connection of agglomerates. Meanwhile, M-FeOOH is composed of particles with smaller particle

363 size and shows relatively better dispersion than FeOOH. This indicates that the treatment of micro-

364 wave radiation contributes to improving the dispersion of particles formed on the catalyst surface.

365 Interestingly, the cyclic tests for five times almost does not affect the morphology of the catalyst

366 apart from the appearing of a slight aggregation of small particles on the surface of Spent-M-FeOOH.

367 This confirms the good stability of the iron hydroxide catalyst treated by microwave radiation.

368 **Table 2** The physical structural parameters of FeOOH, M-FeOOH and Spent-M-FeOOH catalysts

Catalysts	BET surface area [a] (m^2/g)	Pore volume [b] (cm^3/g)	Pore diameter [c] (nm)	average particle size (μm)
FeOOH	259.6	0.26	3.27	4.36
M-FeOOH	240.7	0.27	3.42	3.85
Spent-M-FeOOH	161.5	0.15	3.38	/

369 a BET surface area. b BJH desorption pore volume. c BJH desorption pore diameter

370 According to the IUPAC classification and the results of N_2 adsorption-desorption in Fig.4(d)-

371 (e) and Table 2, the FeOOH and M-FeOOH catalysts exhibit the type IV isotherm with a H1 hyste-

372 resis loop appearing in the high-pressure region, indicating the presence of mesoporous structure

373 with uniformly distribution [21,45,49,50]. Meanwhile, the treatment of microwave radiation can make

374 the low-pressure closing point of N_2 adsorption-desorption isotherm to shift to right slightly, demon-

375 strating that this treatment might be unhelpful to the pore structure due to the desorption and de-

376 composition of partial Fe-OH functional group. Furthermore, the cyclic tests for five times further

377 leads to a shift of the low-pressure closing point of N_2 adsorption-desorption isotherm to high pres-

378 sure. This means that there exists a trend of aggregation and growth of particles under the high

379 alkaline environment of MEA solution, which needs to be further optimized. The calculated data in

380 Table 2 demonstrates that the treatment of microwave radiation decreases the S_{BET} of FeOOH cata-

381 lyst from 259.6 m^2/g to 240.7 m^2/g, but enlarges the pore volume and pore diameter of catalyst,

382 which help facilitate the entry of carbamate into the interior of catalyst for the reaction. Furthermore,

383 the Spent-M-FeOOH catalyst after five cyclic tests still has 161.5 m^2/g of S_{BET} and 3.38 nm of pore

384 diameter, which are also considerable to the catalytic desorption of CO_2. At the same time, the re-

385 sults in Fig.S5 and Table 2 demonstrate that the treatment of microwave radiation indeed regulates

386   the particle size distribution of FeOOH catalyst and leads to a more concentrated bimodal distribu-

387   tion, which reduces the average particle size of FeOOH catalyst.

388   **3.2 Catalytic desorption performance**
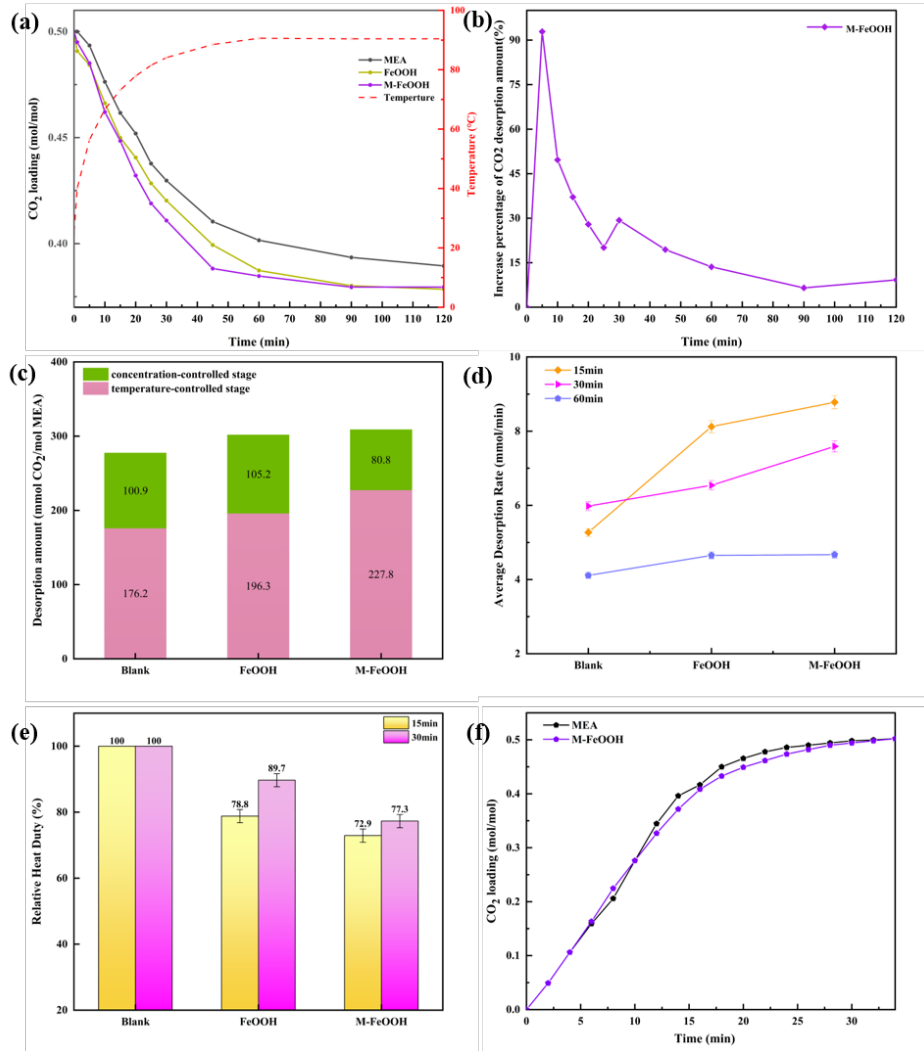
389

390   **Fig.5** The CO_2 desorption performance over the catalysts: (a) The desorption curves of CO_2 (b) Percentage in-

391   crease in CO_2 desorption amount after the addition of M-FeOOH catalyst (c) The desorption amount of CO_2 during

392   the temperature control phase and concentration control phase (d) 15 min, 30 min and 60 min average desorption

393   rates (e) 15 min and 30 min relative heat duties (f) Influence of M-FeOOH catalyst on the absorption of CO_2

394   In order to study the influence of microwave radiation treatment on the catalytic desorption of

395   CO_2 over the FeOOH catalyst, a series of experiments were carried out by using the flake catalyst

396   and the parameters, including the desorbed quantities of CO_2 (n_{CO2}), the average desorption rate (r),

397   the relative heat duty (RHD), the heat duty (HD) and the desorption parameter (DP). Based on the

398   curves of CO_2 loading in MEA solution at desorption temperatures of 40-90 °C in Fig.5(a) and Table

399 S2, it can be found that the FeOOH catalyst presents good catalytic performance for the regeneration

400 of MEA solution and reduces the loading of CO_2 effectively in it. Furthermore, the treatment of

401 microwave radiation further accelerates the desorption rate of CO_2 during the heating stage, thus

402 the percentage increase of CO_2 desorption amount was calculated to investigate the effect of M-

403 FeOOH catalyst at the initial stage.

404   As shown in Fig.5(b), it is observed that the introduction of M-FeOOH catalyst can achieve a

405 peak increase rate of 92% in the desorption amount of CO_2 relative to the blank group at the 10 th

406 minute. The process of CO_2 desorption from MEA solution is divided into two stages including the

407 temperature control stage (first 30 minutes) and the concentration control stage (next 90 minutes).

408 It is clear that the introduction of iron hydroxide catalyst indeed increases the desorption amount of

409 CO_2 at the temperature control stage, especially M-FeOOH. Furthermore, the total amount of CO_2

410 desorption within 120 minutes over M-FeOOH catalyst is slightly larger than that of FeOOH, which

411 indicates that the treatment of microwave radiation optimizes the catalytic regeneration of MEA

412 solution over FeOOH catalyst, especially increasing the desorption rate of CO_2 at the temperature

413 control stage. According to the calculated average desorption rates of CO_2 in Fig.5(c), the applica-

414 tion of M-FeOOH catalyst increases the average desorption rate in the first 15 minutes by 8% and

415 66.6% compared to FeOOH catalyst and the blank group, respectively. Fig.5(e) gives the effect of

416 FeOOH and M-FeOOH catalysts on the relative heat duty of CO_2 desorption from MEA solution in

417 the first 15 minutes or 30 minutes. It can be found that the introduction of iron hydroxide catalyst

418 reduces the relative heat duty of CO_2 desorption effectively, and the relative heat duty in the first 15

419 minutes is decreased separately by 21.2% and 27.1% for FeOOH and M-FeOOH catalysts, which

420 is consistent with the law of average desorption rate. In addition, M-FeOOH maintains high activity

421 in the first 30 minutes and reduces the relative heat duty by 12.4% compared to FeOOH catalyst.

422 According to the results of CO_2 absorption in MEA solution in Fig.5(d), it can be found that the

423 application of M-FeOOH catalyst will not affect the absorption of CO_2 in MEA solution, or im-

424 proves the absorption rate in the first 10 minutes. Considering both the desorption rate and heat duty,

425 the desorption parameters were calculated to evaluate the introduction of M-FeOOH catalyst on the

426 regeneration of MEA solution. As depicted in Fig.S4, the desorption parameter increases with the

427 enhancement of catalyst amount from 0.2 wt.% to 0.8 wt.%, which is enhanced by 35% when the

428 used amount of catalyst increases from 0.2 wt.% to 0.4 wt.%, and the suitable amount of M-FeOOH

429   is 0.4 wt.%. Furthermore, the catalytic performance of CO_2 desorption from MEA solution over

430   different solid acid catalysts were given in Table S1 for comparison. It can be found that the as-

431   prepared M-FeOOH catalyst increases the amount of CO_2 desorption and reduces the renewable

432   energy consumption at the temperature of 90 $^{\circ}C$ effectively, which is better than the most reported

433   solid acid catalysts in table S1.
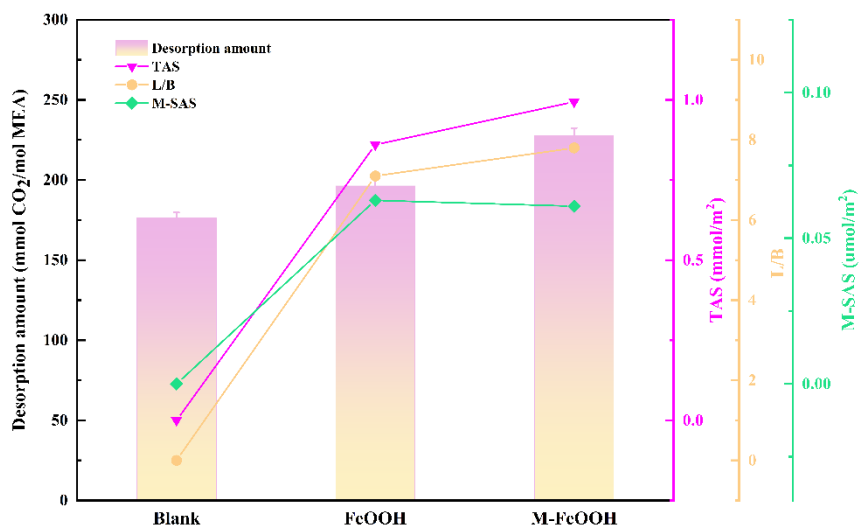
434

435   **Fig.6** Correlation of CO_2 desorption amount with acid site distribution and specific surface area of catalysts

436   Based on the same desorption time and power consumption, the desorbed amount of CO_2 can

437   be visualized as a response to the relative magnitude of the heat duty, thus the relationship of the

438   desorbed amount of CO_2 with the molar ratio of surface Lewis and Bronsted acid sites(L/B), the

439   total acid sites (TAS) and medium-strong acid sites(M-SAS) per unit surface area are represented in

440   Fig.6. As shown in Fig.6, the desorbed amount of CO_2 is positively correlated with the molar ratio

441   of surface Lewis and Bronsted acid sites(L/B) and the total acidic sites per unit surface area (TAS),

442   but is weakly related to the Medium-strong acidic sites per surface area owing to the slightly lower

443   calculated value of M-SAS for M-FeOOH catalyst although it has better catalytic performance of

444   CO_2 desorption than FeOOH. Previous researches pointed out that the effect of catalyst became

445   mainly to assist the reaction between $MEAH^+$ and $MEACOO^-$ as the enhancement of CO_2 desorp-

446   tion and solution alkalinity [51]. Wherein, Bronsted acid sites contributes to providing the proton for

447   the dissociation of carbamate, while Lewis acid sites principally accept the electrons to assist the

448   recovery of $MEAH^+$ [28,30,51]. However, higher activation energy needs to overcame for the de-pro-

449   tonation reaction of $MEAH^+$ than the dissociation of carbamate, which might explain the promo-

450   tional effect of L/B ratio enhancement on the catalytic desorption of CO_2 from MEA solution over

451   the as-prepared FeOOH catalyst [28,39,51].

452   The stability of catalyst is an important parameter for the regeneration of MEA solution and

453   needs to be studied, thus five cyclic experiments were conducted on the desorption of CO_2 over the

454   M-FeOOH catalyst. During this experiment, the flake catalyst was taken out of the MEA solution

455   every time after the desorption of CO_2 and washed completely to remove the adsorbed amine on the

456   catalyst surface with de-ionized water, and then dried before the next cyclic test. As shown in Fig.7,

457   around 224 mmol/mol of CO_2 desorption amount and 78.5% of the relative heat duty achieve in the

458   first 30 min for the M-FeOOH catalyst after being tested for four cycles, which are close to the

459   activity of the fresh catalyst. This indicates that the iron hydroxide catalyst synthesized by micro-

460   wave radiation assisted preparation method presents a good stability on the catalytic desorption of

461   CO_2 from MEA solution. The results of characterizations in Section 3.1 demonstrate that Spent-M-

462   FeOOH exhibits similar iron-based crystals, surface functional groups and morphology to fresh M-

463   FeOOH, which also confirms the excellent stability of the synthesized catalyst in this study. Fur-

464   thermore, the cyclic tests contribute to adjust the electron cloud density around iron element and the

465   surface acid sites of catalyst, thereby improve the surface oxygen vacancies and weak acid sites of

466   M-FeOOH due to the adsorption of water and the residue of MEA on the catalyst surface although

467   the obtained Spent-M-FeOOH catalyst was washed thoroughly with de-ionized water. Meanwhile,

468   this residue might decrease the BET surface area of catalyst, which needs to be optimized in further

469   studies.
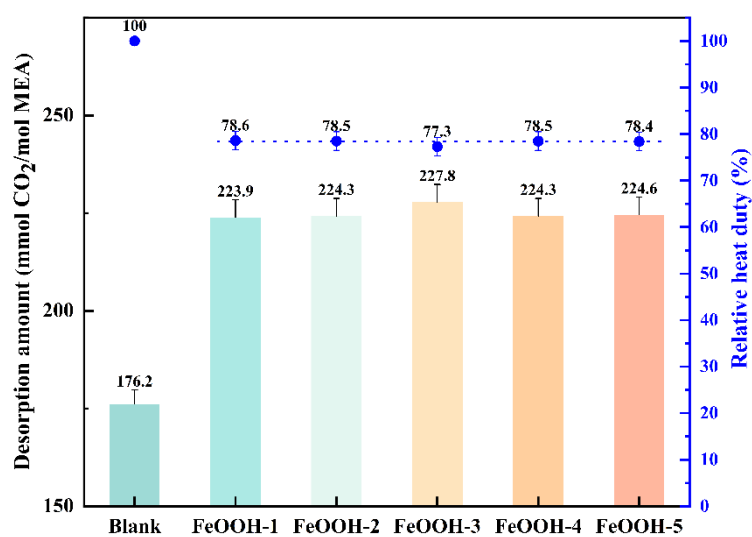
470

471   **Fig.7** Cyclic stability tests of the catalytic CO_2 desorption from MEA solution over M-FeOOH catalyst

472   **3.3 DFT calculations**
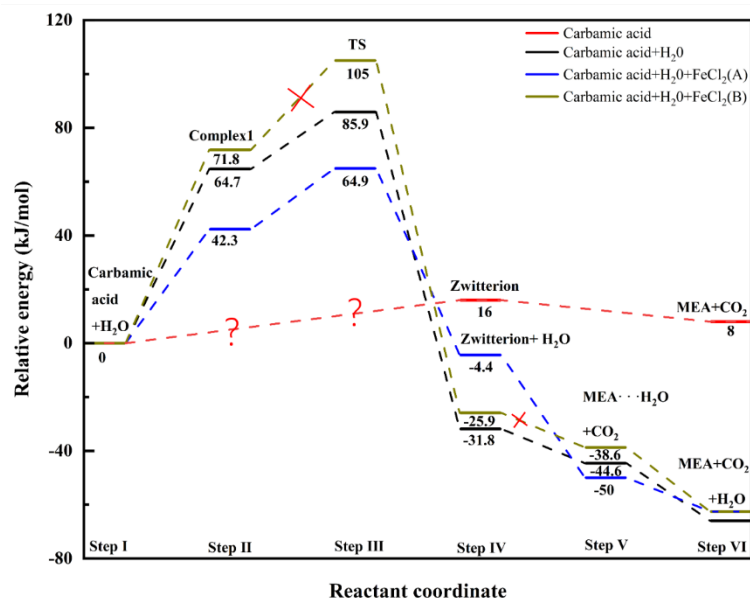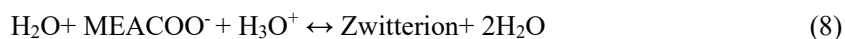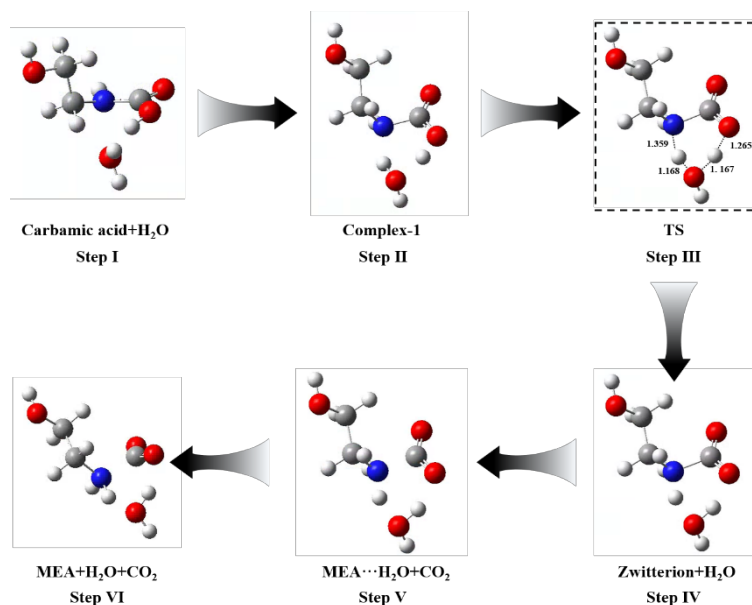
Fig.8 Potential energy plots of isomerization processes assisted by water or/and iron catalyst for carbamic acid

The zwitterion mechanism of CO_2 desorption is the reverse reaction of absorption, which can be divided into two main parts, the decomposition of carbamate and the deprotonation of protonated amine [52]. The protonated amines transfer protons to H_2O and HCO_3^{2-}, which act as the intermediate carriers to transfer protons to carbamates to form carbamic acid. And through the process of isomerization, protons are transferred from O to N atoms to form zwitterions, and then the C-N bonds are broken to form MEA and CO_2. There exists the key step of an isomerization reaction for the mechanisms proposed for the desorption of CO_2 from MEA solution [20,21,49]. Because the N atom of carbamate might be directly attacked by the protons from strong acid sites (e.g., SO_4^{2-}) in alkaline amine solution [54], while the protons from weak and medium-strong acid sites preferentially combine with more electronegative oxygen atoms to form carbamate, and an isomerization reaction is sure to occur [6,20,27]. However, less researches have been investigated in the isomerization process of CO_2 desorption from MEA solution. In this study, the reactants, transition states, intermediate states and products of the isomerization were simulated using Gaussian 16w to unveil this process and the effect of water or/and iron catalyst ($FeCl_2$) have also been investigated with the relative energies calculated correspondingly.

The potential energy plot (PES) of MEACOOH-H_2O in CO_2-loaded MEA solution were obtained based on the IEFPCM model [55], vesicle radius and B3LYP/6-311G (d, p) level and the results are given in Fig.8. It can be found that there exist two possible paths for the isomerization process of carbamic acid by analyzing the computed infrared spectra, which are the vibration peak of H

494   atom to N atom at 1186.6 cm^{-1} and the vibration peak for the departure of H atom from O atom at

495   3766.4 cm^{-1}, respectively. Herein, a display water molecule was introduced and found that there

496   exist blue shift and red shift separately for the vibration peaks of H atom to N atom and H atom to

497   O atom, and their intensities also increase by a factor of 1.3 and 8.2, respectively. This indicates that

498   H atom is easier to detach from carbamic acid and binds with water compared to the vibration peak

499   of H atom to N atom. Therefore, in this study, water molecule was introduced to participate in the

500   isomerization reaction, which helped to convert the original intramolecular proton transfer into the

501   molecule-to-molecule proton transfer. As shown in Fig. 8, the relative energies of the isomerization

502   reaction could not be quantified in the absence of water molecule, and there exists an energy barrier

503   of 16 kJ/mol between zwitterion and carbamic acid, resulting in a huge energy requirement for the

504   reaction. However, the isomerization reaction at the presence of water exhibits an energy barrier of

505   only 85.9 kJ/mol, and the energies after the transition states are all progressively lower and negative,

506   demonstrating that the subsequent reaction can proceed spontaneously as long as the energy barrier

507   is crossed. The specific reaction paths for the isomerization of carbamic acid is given in Fig.9, and

508   it can be found that at the presence of water, the H atom of carbamic acid is first strongly attracted

509   to the O atom of water(Step Ⅰ), but its other H atom slowly breaks off as the H atom gradually

510   approaches H$_2$O(Step Ⅱ), at which point a stable hexagon is formed between the H-O-H of water

511   and the N-C-O of carbamate(Step Ⅲ), wherein the lengths of N-H and O-H bonds are 1.36 Å and

512   1.26 Å respectively. Subsequently, the O atom gives its combined H atom to the N atom by bonding

513   with the foreign H atom and a zwitterion is formed due to the combination of N and H atoms (Step

514   Ⅳ). Finally, the C-N bond breaks to form MEA and CO$_2$ (Step Ⅴ and Ⅵ) (Eqs. (8) and (9)). Thus,

515   it can be inferred that more water molecules contribute to improve the isomerization reaction by

516   reducing the energy requirements significantly.

$$H_2O + MEACOO^- + H_3O^+ \leftrightarrow Zwitterion + 2H_2O \tag{8}$$

$$Zwitterion \leftrightarrow MEA + CO_2 \tag{9}$$

$$Fe-O^- + MEAH^+ \leftrightarrow MEA + Fe-OH \tag{10}$$

$$H_2O + Fe-OH + MEACOO^- \rightarrow MEAH^+COO^- + Fe-O^- + H_2O \tag{11}$$

Fig.9 Simulation results of water-assisted isomerization reaction mechanism with bond lengths in angstroms

It should be mentioned that three active centers (one N atom and two O atoms) are exposed for carbamate acid [28]. Among them, the atom of N usually serves as a crucial active center for the decomposition of carbamate, but its location within the structure leads N atom less readily adsorbed on the introduced catalyst surface in the isomerization reaction [56]. Therefore, Fe^{2+} of ferrous chloride was chosen as the unsaturated metal (LAS) active sites to simulate the adsorption of two activate oxygen from carbamic acid on the surface of FeOOH catalyst. As depicted in Fig. 8 and 10, the oxygen active center of the absorbed CO_2 in carbamic acid is easily bound together to the Fe atoms of the introduced iron-based catalyst via Eqs. (10) and (11), which decreases the energy barrier of isomerization reaction to 64.9 kJ/mol at the presence of water, representing a reduction of 24.5%. Furthermore, it can be observed that along the specific reaction path under the action of iron-based catalyst, the bonds of both O-H and N-H in transition states elongate to 1.56 Å and 1.57 Å, respectively. This causes the originally stable hexagonal ring to become more stable and reduces the reaction energy barrier, which is consistent with the experimental catalytic mechanisms of CO_2 desorption in previous literatures [20,21,32]. In addition, only 2.8 kJ/mol of energy is required to the fracture of Fe-O, and the introduction of iron-based catalyst reduces the activation energy of the isomerization effectively, but it does not alter the free energy of reactants/products.
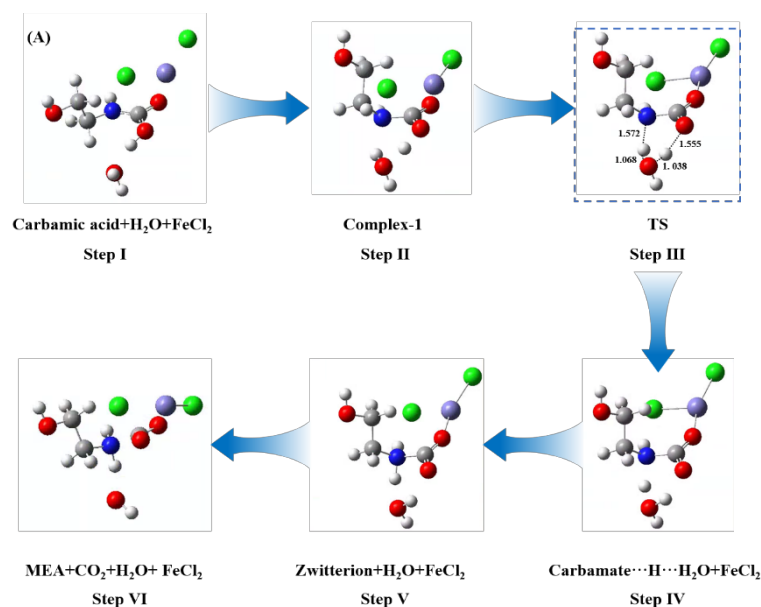
Fig.10 Simulation results on the mechanism of isomerization reaction assisted by the combination of water and Fe-based catalyst (bond lengths in angstroms)

The calculated energy barriers and specific reaction path in the case that the other oxygen active center directly from carbamic acid rather than the absorbed CO_2, is bound together to the Fe atoms of the introduced iron-based catalyst, are given in Fig.8 and Fig.S5. It can be found that the bind of Fe atoms to the oxygen active center directly from carbamic acid increases the reaction energy barrier of isomerization reaction by 22.1%. Furthermore, in this specific reaction path, the position of CO_2 rotates by 90° compared to the reaction via the formed bond of Fe atom with the oxygen active center of the absorbed CO_2 in carbamic acid, which results in a more unstable structure of transition state and instead increases the energy barrier of isomerization reaction. Therefore, it can be inferred that the Fe atoms of the introduced iron-based catalyst should bind with the oxygen active center of the absorbed CO_2 in carbamic acid, thereby reducing the reaction energy barrier of isomerization reaction and promoting the regeneration of MEA. Finally, based on the calculation results in this research, the detailed reaction path of CO_2 desorption and the regeneration mechanism of MEA over the iron-based catalyst are proposed and given in Fig.11. Firstly, the introduced iron-based catalyst carries the protons of $MEAH^+$ or/and supply its own inherent protons to participate in the decomposition reaction of carbamate by converting $MEACOO^-$ into MEACOOH. Subsequently, the Lewis acid site of iron-based catalyst attacks and adsorbs the oxygen active center of the absorbed CO_2 in carbamic acid and thus MEACOOH is fixed on the catalyst surface. And then, the molecule of water in aqueous solution participates in the reaction of isomerization and transfers the protons from the

O atom to the N atom in carbamate acid. During this reaction process of isomerization, the formation

and breaking of bond undergo for the molecule of water, and then the acid site of catalyst removes

the lone pair electrons of the N atom for carbamate and makes its configuration change from sp2

hybrid to sp3 hybrid orbital, and a zwitterion is formed. Finally, the C-N bond of the zwitterion is

elongated and then its break leads to the formation of CO_2/H_2O and the regeneration of MEA/Cat-

alyst. At the same time, it should also be mentioned that the abundant acid sites of iron-based catalyst

also contribute to provide protons for the decomposition reaction of HCO_3^{3-}/CO_3^{2-} into H_2O and CO_2.
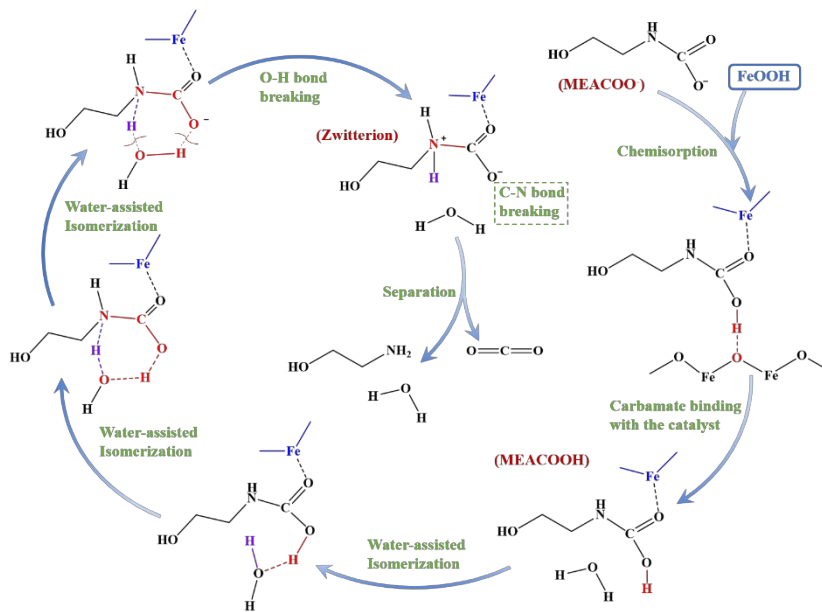
Fig.11 Mechanism of CO_2 desorption from CO_2-loaded MEA solution over Fe-based catalyst

4 Conclusions

In this study, microwave radiation had been applied to increase the catalytic desorption of CO_2

from CO_2-loaded MEA solution over the iron hydroxide catalyst, which was found to further accel-

erate the CO_2 desorption rate at the heating stage and decrease the relative desorption heat duty of

FeOOH catalyst, and the M-FeOOH catalyst presents a good stability for CO_2 desorption. The treat-

ment of microwave radiation leads to the decomposition of partial Fe-OH functional group of iron

hydroxide and promotes the lattice transitions from β-FeOOH to α-FeOOH, which decreases the

BET surface area and weak acid sites of FeOOH catalyst slightly, but increases the dispersion, me-

dium-strong acid sites and pore volume of catalyst. Furthermore, this treatment reduces the calcu-

lated surface molar ratio of lattice hydroxyls/(lattice oxygen + lattice hydroxyls), but the cyclic test

helps to the formation of hydroxyl oxygen from the adsorbed water, which plays an important role

on the regeneration of MEA solution. The results of DFT calculation indicate that water molecule

indeed contributes to converting the original intra-molecular proton transfer into the molecule-to-molecule proton transfer in the reaction of isomerization actively. Finally, the influence of iron-based catalyst on the isomerization of MEA solution are calculated by choosing Fe^{2+} of ferrous chloride as the unsaturated metal (LAS) active sites to simulate the adsorption of carbamic acid, and found that the adsorption of LAS and uniformly dispersed active sites of iron-based catalyst contributed to providing an advantageous condition for the decomposition of carbamate and promoting the regeneration of MEA.

CRediT authorship contribution statement

Haoran Zhang: Writing - original draft, Methodology, Validation. **Junge Lv:** Validation and Methodology. **Zhibo Xiong:** Conceptualization, Funding acquisition, Writing - review & editing. **Huancong Shi and Jing Jin:** Investigation, Supervision, Writing - review & editing, Funding acquisition. **Mengqi Liu, Yanping Du** and **Wei Lu:** Investigation, Supervision and editing.

Declaration of Competing Interest

The authors declare that they have no known competing financial interests or personal relationships that could have appeared to influence the work reported in this paper.

Acknowledgements

References

[1] Z. Liang, W. Rongwong, H. Liu, K. Fu, H. Gao, F. Cao, R. Zhang, T. Sema, A. Henni, K. Sumon, D. Nath, D. Gelowitz, W. Srisang, C. Saiwan, A. Benamor, M. Al-Marri, H. Shi, T. Supap, C. Chan, Q. Zhou, M. Abu-Zahra, M. Wilson, W. Olson, R. Idem, P. Tontiwachwuthikul, Recent progress and new developments in post-combustion carbon-capture technology with amine based solvents, Int. J. Greenhouse Gas Control. 40 (2015) 26-54, http://doi.org/10.1016/j.ijggc.2015.06.017.

[2] M. McNutt, Time's up, CO_2, Science 365 (2019) 411, http://doi.org/10.1126/science.aay8827.

[3] W.D. Jones, Carbon Capture and Conversion, J. Am. Chem. Soc. 142 (2020) 4955-4957, http://doi.org/10.1021/jacs.0c02356.

[4] W. Gao, S. Liang, R. Wang, Q. Jiang, Y. Zhang, Q. Zheng, B. Xie, C. Ying, X. Zhu, J. Wang, L. Huang, Y.

606   shan, Z. Wang, C. Jo, Q. Wang, L. Wang, Y. Liu, B. Louis, J. Scott, A. Roger, R. Amal, H. He, S. Park, Industrial

607   carbon dioxide capture and utilization: state of the art and future challenges, Chem. Soc. Rev. 49 (2020) 8584-

608   8686, http://doi.org/10.1039/d0cs00025f.

609   [5]   H. Gao, Y. Huang, X. Zhang, Z.A.S. Bairq, Y. Huang, P. Tontiwachwuthikul, Z. Liang, Catalytic performance

610   and mechanism of SO_4^{2-}/ZrO_2/SBA-15 catalyst for CO_2 desorption in CO_2-loaded monoethanolamine solution,

611   Appl. Energy 259 (2020) 114179, http://doi.org/10.1016/j.apenergy.2019.114179.

612   [6]   T. Li, Q. Yu, F. Barzagli, C. Li, M. Che, Z. Zhang, R. Zhang, Energy efficient catalytic CO_2 desorption:

613   mechanism, technological progress and perspective, Carbon Capture Sci. Technol. 6 (2023) 100099,

614   http://doi.org/10.1016/j.ccst.2023.100099.

615   [7]   C. Yu, H. Ling, W. Cao, F. Deng, Y Zhao, D Cao, M. Tie, X Hu, Revealing the potential of cyclic amine

616   morpholine (MOR) for CO_2 capture through a comprehensive evaluation framework and rapid screening

617   experiments, Chem. Eng. J. 495 (2024) 153402, http://doi.org/10.1016/j.cej.2024.153402.

618   [8]   F. Meng, Y. Meng, T. Ju, S. Han, L. Lin, J. Jiang, Research progress of aqueous amine solution for CO_2 capture:

619   A review, Renewable and Sustainable Energy Rev. 168 (2022) 112902,

620   http://doi.org/10.1016/j.rser.2022.112902.

621   [9]   X. Li, L. Xing, G Zhan, Z. Huang, Z. Chen, H. Chang, J. Li, Oxygen Vacancy Enhanced Proton Transfer to

622   Boost Carbamate Decomposition Kinetics with Tunable Heterostructure Ni/NiO, ACS Catal. 14 (2024) 1083-

623   1092, http://doi.org/10.1021/acscatal.3c03852.

624 [10]   M.S. Alivand, O. Mazaheri, Y. Wu, A. Zavabeti, A.J. Christofferson, N. Meftahi, S.P. Russo, G.W. Stevens,

625   C.A. Scholes, K.A. Mumford, Engineered assembly of water-dispersible nanocatalysts enables low-cost and

626   green CO_2 capture, Nat. Commun. 13 (2022) 1249, http://doi.org/10.1038/s41467-022-28869-6.

627 [11]   K. Wei, L. Xing, Y. Li, T. Xu, Q. Li, L. Wang, Heteropolyacid modified Cerium-based MOFs catalyst for

628   amine solution regeneration in CO_2 capture, Sep. Purif. Technol. 293 (2022) 121144,

629   http://doi.org/10.1016/j.seppur.2022.121144.

630 [12]   A.F. Mohammad, A.A-H. Mourad, A.H. Al-Marzouqi, M.H. El-Naas, B.V. Bruggen, M.H. Al-Marzouqi,

631   Multistage modified Solvay process based on calcium oxide for carbon dioxide capture and reject brine

632   desalination, Sep. Purif. Technol. 328 (2024) 125000, http://doi.org/10.1016/j.seppur.2023.125000.

633 [13]   C. Yu, H. Ling, Z. Shen, H. Yang, D. Cao, X. Hu, A general model for prediction of the CO_2 equilibrium

634   solubility in aqueous tertiary amine systems, AIChE J. (2024) e18551, http://doi.org/10.1002/aic.e18551.

635 [14] G.T. Rochelle, Amine Scrubbing for CO_2 Capture, Science. 325 (2009) 1652-1654, http://doi.org/10.1126/science.1176731.

637 [15] A. Akachuku, P.A. Osei, B. Decardi-Nelson, W. Srisang, F. Pouryousefi, H. Ibrahim, R. Idem, Experimental and kinetic study of the catalytic desorption of CO_2 from CO_2-loaded monoethanolamine (MEA) and blended monoethanolamine - Methyl-diethanolamine (MEA-MDEA) solutions, Energy. 179 (2019) 475-489, http://doi.org/10.1016/j.energy.2019.04.174.

641 [16] K. Xue, G. Zhan, X. Wu, H. Zhang, Z. Chen, H. Chen, J. Li, Integration of membrane contactors and catalytic solvent regeneration for efficient carbon dioxide capture, J. Membr. Sci. 684 (2023) 121870, http://doi.org/10.1016/j.memsci.2023.121870.

644 [17] Y. Guo, H. Zhang, K. Fu, X. Chen, M. Qiu, Y. Fan, Integration of solid acid catalyst and ceramic membrane to boost amine-based CO_2 desorption, Energy 274 (2023) 127329, http://doi.org/10.1016/j.energy.2023.127329.

647 [18] M.S. Alivand, O. Mazaheri, Y. Wu, G.W. Stevens, C.A. Scholes, K.A. Mumford, Catalytic Solvent Regeneration for Energy-Efficient CO_2 Capture, ACS Sustainable Chem. Eng. 8 (2020) 18755-18788, http://doi.org/10.1021/acssuschemeng.0c07066.

650 [19] Z. Tan, S. Zhang, F. Zhao, R. Zhang, F. Tang, K. You, H. Luo, X. Zhang, SnO_2/ATP catalyst enabling energy-efficient and green amine-based CO_2 capture, Chem. Eng. J. 453 (2023) 13980, http://doi.org/10.1016/j.cej.2022.139801.

653 [20] M. Waseem, M. Al-Marzouqi, N. Ghasem, A review of catalytically enhanced CO_2-rich amine solutions regeneration, J. Environ. Chem. Eng, 11 (2023) 110188, http://doi.org/10.1016/j.jece.2023.110188.

655 [21] R. Zhang, T. Li, Y. Zhang, J. Ha, Y. Xiao, C. Li, X. Zhang, H. Luo, CuO modified KIT-6 as a high-efficiency catalyst for energy-efficient amine solvent regeneration, Sep. Purif. Technol. 300 (2022) 121702, http://doi.org/10.1016/j.seppur.2022.121702.

658 [22] Z. Yang, Y. Shen, H. Yang, H. Yi, H. Guo, X. Zhang, A review of CO_2 catalytic regeneration research based on MEA solution, Front. Energy Res. 11 (2023) 1257218, http://doi.org/10.3389/fenrg.2023.1257218.

660 [23] S. An, T. Xu, L. Xing, G. Yu, R. Zhang, J. Liu, A. Aierken, Q. Dai, L. Wang, Recent progress and prospects in solid acid-catalyzed CO_2 desorption from amine rich liquid, Gas Sci. Eng. 120 (2023) 205152, http://doi.org/10.1016/j.jgsce.2023.205152.

663 [24] U.H. Bhatti, D. Sivanesan, D.H. Lim, S.C. Nam, S. Park, I.H. Baek, Metal oxide catalyst-aided solvent regeneration: A promising method to economize post-combustion CO_2 capture process, J. Taiwan Inst. Chem.

665   Eng. 93 (2018) 150-157, http://doi.org/10.1016/j.jtice.2018.05.029.

666 [25] U.H. Bhatti, S. Nam, S. Park, I.H. Baek, Performance and Mechanism of Metal Oxide Catalyst-Aided Amine

667   Solvent Regeneration, ACS Sustainable Chem. Eng. 6 (2018) 12079-12087,

668   http://doi.org/10.1021/acssuschemeng.8b02422.

669 [26] U.H. Bhatti, A.K. Shah, J.N. Kim, J.K. You, S.H. Choi, D.H. Lim, S. Nam, Y.H. Park, I.H. Baek, Effects of

670   Transition Metal Oxide Catalysts on MEA Solvent Regeneration for the Post-Combustion Carbon Capture

671   Process, ACS Sustainable Chem. Eng. 5 (2017) 5862-5868, http://doi.org/10.1021/acssuschemeng.7b00604.

672 [27] A.H. Bhatti, M. Waris, W.W. Kazmi, U.H. Bhatti, G.H. Min, B.C. Park, S. Kweon, I.H. Baek, Sung Chan Nam,

673   Metal impregnated activated carbon as cost-effective and scalable catalysts for amine-based CO_2 capture, J.

674   Environ. Chem. Eng. 11 (2023) 109231, http://doi.org/10.1016/j.jece.2022.109231.

675 [28] X. Zhang, Y. Huang, J. Yang, H. Gao, Y. Huang, X. Luo, Z. Liang, P. Tontiwachwuthikul, Amine-based CO_2

676   capture aided by acid-basic bifunctional catalyst: Advancement of amine regeneration using metal modified

677   MCM-41, Chem. Eng. J. 383 (2020) 123077, http://doi.org/10.1016/j.cej.2019.123077.

678 [29] Y. Li, Z. Chen, G. Zhan, B. Yuan, L. Wang, J. Li, Inducing efficient proton transfer through Fe/Ni@COF to

679   promote amine-based solvent regeneration for achieving low-cost capture of CO_2 from industrial flue gas, Sep.

680   Purif. Technol. 298 (2022) 121676, http://doi.org/10.1016/j.seppur.2022.121676.

681 [30] L. Xing, K. Wei, Q. Li, R. Wang, S. Zhang, L. Wang, One-Step Synthesized SO_4^{2-}/ZrO_2-HZSM-5 Solid Acid

682   Catalyst for Carbamate Decomposition in CO_2 Capture, Environ. Sci. Technol. 54 (2020) 13944-13952,

683   http://doi.org/10.1021/acs.est.0c04946.

684 [31] Q. Lai, S. Toan, M.A. Assiri, H. Cheng, A.G. Russell, H. Adidharma, M. Radosz, M. Fan, Catalyst-$TiO(OH)_2$

685   could drastically reduce the energy consumption of CO_2 capture, Nat. Commun. 9 (2018) 2672,

686   http://doi.org/10.1038/s41467-018-05145-0.

687 [32] C. Jiang, M. Fan, G. Gao, W. Jiang, X. Li, C. Luo, L. Zhang, F. Wu, Nanostructured AlOOH – A promising

688   catalyst to reduce energy consumption for amine-based CO_2 capture, Sep. Purif. Technol. 303 (2022) 122232,

689   http://doi.org/10.1016/j.seppur.2022.122232.

690 [33] L. Ji, J. Li, R. Zhai, J. Wang, X. Wang, S. Yan, M. Hua, Metal Oxyhydroxide Catalysts Promoted CO_2

691   Absorption and Desorption in Amine-Based Carbon Capture: A Feasibility Study, ACS Omega. 7 (2022)

692   44620-44630, http://doi.org/10.1021/acsomega.2c02851.

693 [34] J. Hu, S. Li, J. Chu, S. Niu, J. Wang, Y. Du, Z. Li, X. Han, P. Xu, Understanding the Phase-Induced

694   Electrocatalytic Oxygen Evolution Reaction Activity on FeOOH Nanostructures, ACS Catal. 9 (2019) 10705-

695   10711, http://doi.org/10.1021/acscatal.9b03876.

696 [35] Z. Xiong, C. Wu, Q. Hu, Y. Wang, J. Jin, C. Lu, D. Guo, Promotional effect of microwave hydrothermal

697   treatment on the low-temperature NH_3-SCR activity over iron-based catalyst, Chem. Eng. J. 286 (2016) 459-

698   466, http://doi.org/10.1016/j.cej.2015.10.082.

699 [36] S. Yang, C. Wang, L. Chen, S. Chen, Facile dicyandiamide-mediated fabrication of well-defined CuO hollow

700   microspheres and their catalytic application, Mater. Chem. Phys. 120 (2010) 296-301,

701   http://doi.org/10.1016/j.matchemphys.2009.11.005.

702 [37] Y. Zhang, K. Li, J. Liao, X. Wei, L. Zhang, Microwave-assisted synthesis of graphitic carbon nitride/CuO

703   nanocomposites and the enhancement of catalytic activities in the thermal decomposition of ammonium

704   perchlorate, Appl. Surf. Sci. 499 (2020) 143875, http://doi.org/10.1016/j.apsusc.2019.143875.

705 [38] H. Shi, J. Fu, Q. Wu, M. Huang, L. Jiang, M. Cui, R. Idem, P. Tontiwachwuthikul, Studies of the coordination

706   effect of DEA-MEA blended amines (within $1+4$ to $2+3$ M) under heterogeneous catalysis by means of

707   absorption and desorption parameters, Sep. Purif. Technol. 236 (2020) 116179,

708   http://doi.org/10.1016/j.seppur.2019.116179.

709 [39] B. Guo, H. Huo, Q. Zhuang, X. Ren, X. Wen, B. Yang, X. Huang, Q. Chang, S. Li, Iron Oxyhydroxide:

710   Structure and Applications in Electrocatalytic Oxygen Evolution Reaction, Adv. Funct. Mater. 33 (2023)

711   230057, http://doi.org/10.1002/adfm.202300557.

712 [40] L. Liu, H. Chen, E. Shiko, X. Fan, Y. Zhou, G. Zhang, X. Luo, X. Hu, Low-cost DETA impregnation of acid-

713   activated sepiolite for CO_2 capture, Chem. Eng. J. 353 (2018) 940-948,

714   http://doi.org/10.1016/j.cej.2018.07.086.

715 [41] M.C. Kimling, N. Scales, T.L. Hanley, R.A. Caruso, Uranyl-Sorption Properties of Amorphous and Crystalline

716   TiO_2/ZrO_2 Millimeter-Sized Hierarchically Porous Beads, Environ. Sci. Technol. 46 (2012) 7913-7920,

717   http://doi.org/10.1021/es3011157.

718 [42] C. Wang, A. Li, C. Shuang, The effect on ozone catalytic performance of prepared-FeOOH by different

719   precursors, J. Environ. Manage. 228 (2018) 158-164, http://doi.org/10.1016/j.jenvman.2018.08.103.

720 [43] Y. Li, Z. Chen, B. Yuan, L. Xing, G. Zhan, Y. Peng, L. Wang, J. Li, Synergistic promotion for CO_2 absorption

721   and solvent regeneration by fine waste red mud particles on in amine-based carbon capture: Performance and

722   mechanism, Sep. Purif. Technol. 304 (2023) 122380, http://doi.org/10.1016/j.seppur.2022.122380.

723 [44] D. Ye, R. Wang, X. Wang, X. Liu, H. Liu, H. Wang, Improvement in the Hg0 removal performance of CeO_2

724   by modifying with CuO, Appl. Surf. Sci. 579 (2022) 152200, http://dx.doi.org/10.1016/j.apsusc.2021.152200.

[45] X. Yang, R. Zhou, G. Liu, S. Hussain, Q. Li, Reduce energy consumption for organic amine regeneration by MnOOH/HZSM-5 catalysts, Chem. Eng. J. 493 (2024) 152564, http://doi.org/10.1016/j.cej.2024.152564.

[46] M. Li, L. Xing, Z. Xu, Z. Liang, T. Qi, Y. Li, S. Zhang, L. Wang, Embedded Mo/Mn Atomic Regulation for Durable Acidity-Reinforced HZSM-5 Catalyst toward Energy-Efficient Amine Regeneration, Environ. Sci. Technol. 57 (2023) 15465-15474, http://doi.org/10.1021/acs.est.3c04916.

[47] Z. Xiong, Z. Sun, J. Liu, Y. Du, Y. Zhu, F. Zhou, J. Jin, Q. Yang, W. Lu, Influence of organic sulfur gas-phase sulfation on the NH_3-SCR activity of CeO_2 catalyst: The competitive adsorption and conversion of CS_2 and COS at a low hydrolysis temperature, Fuel 364 (2024) 131101, http://doi.org/10.1016/j.fuel.2024.131101.

[48] X. Liu, P. Jiang, Y. Chen, Y. Wang, Q. Ding, Z. Sui, H. Chen, Z. Shen, X. Wu, A basic comprehensive study on synergetic effects among the metal oxides in CeO_2-WO_3/TiO_2 NH_3-SCR catalyst, Chem. Eng. J. 421 (2021) 127833, http://doi.org/10.1016/j.cej.2020.127833.

[49] L. Chen, S. Lu, L. Zhang, C. Zhang, L. Liu, G. Kang, H. Tang, S. Chen, Solid Waste of Fly Ash toward Energy-Efficient CO_2 Capture, ACS Sustainable Chem. Eng. 11 (2023) 8281-8293, http://doi.org/10.1021/acssuschemeng.3c00657.

[50] M. Waseem, M. Al-Marzouqi, N. Ghasem, Enhancing regeneration energy efficiency of CO_2-rich amine solution with a novel tri-composite catalyst, J. CO_2 Util. 82 (2024) 102764, http://doi.org/10.1021/j.jcou.2024.102764.

[51] L. Rao, B. Jin, D. Chen, X. Jin, G. Liu, Z. Huang, K. Cao, F. Chen, Q. Huang, Energy-saving CO_2 desorption from amine solution over Fe/SiO_2/biochar catalysts: Desorption performance, structure-activity relationship, and mechanism, Chem. Eng. J. 483 (2024) 149413, http://dx.doi.org/10.1016/j.cej.2024.149413.

[52] X. Hu, L. Liu, X. Luo, G. Xiao, E. Shiko, R. Zhang, X. Fan, Y. Zhou, Y. Liu, Z. Zeng, C. Li, A review of N-functionalized solid adsorbents for post-combustion CO_2 capture, Appl. Energy 260 (2020) 114244, http://doi.org/10.1016/j.apenergy.2019.114244.

[53] R. Zhang, Y. Li, Y. Zhang, T. Li, L. Yang, C. Li, F. Barzagli, Z. Zhang, Energy-Saving Effect of Low-Cost and Environmentally Friendly Sepiolite as an Efficient Catalyst Carrier for CO_2 Capture, ACS Sustainable Chem. Eng. 11 (2023) 4353-4363, http://doi.org/10.1021/acssuschemeng.2c06739.

[54] X. Li, Q. Xu, M. Qi, J. Chen, J. Liu, H. Xie, N. He, S. Chen, Synergistic Catalysis of SO_4^{2-}/TiO_2–CNT for the CO_2 Desorption Process with Low Energy Consumption, ACS Appl. Mater. Interfaces 16 (2024) 26057-26065, http://doi.org/10.1021/acsami.4c01064.

[55] H. Xie, Y. Zhou, Y. Zhang, J. K. Johnson, Reaction Mechanism of Monoethanolamine with CO_2 in Aqueous

755   Solution   from   Molecular   Modeling,   J.   Phys.   Chem.   A   114   (2010)   11844–11852,

756   https://doi.org/10.1021/jp107516k.

757   [56] U.H. Bhatti, A. Ienco, M. Peruzzini, F. Barzagli, Unraveling the Role of Metal Oxide Catalysts in the CO_2

758   Desorption Process from Nonaqueous Sorbents: An Experimental Study Carried out with 13C NMR, ACS

759   Sustainable Chem. Eng. 9 (2021) 15419-15426, http://doi.org/10.1021/acssuschemeng.1c04026.